From MOF membrane to 3D electrode: a new approach toward an electrochemical non-enzymatic glucose biosensor

Yan Zhou, Jie Li, Sasa Wang, Jingtong Zhang & Zixi Kang

Journal of Materials Science
Full Set - Includes `Journal of Materials Science Letters'

ISSN 0022-2461
Volume 52
Number 20

J Mater Sci (2017) 52:12089-12097
DOI 10.1007/s10853-017-1349-2

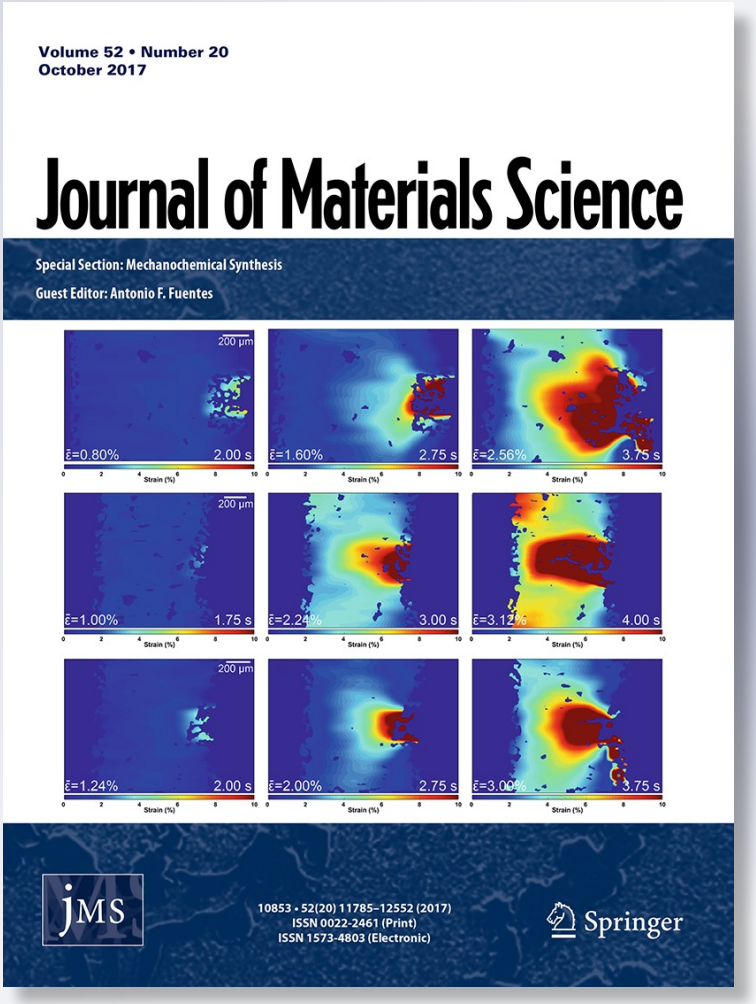

Springer

J Mater Sci (2017) 52:12089–12097

Biomaterials

From MOF membrane to 3D electrode: a new approach toward an electrochemical non-enzymatic glucose biosensor

Yan Zhou[1], Jie Li[2], Sasa Wang[1], Jingtong Zhang[2], and Zixi Kang[1,*]

[1] College of Science, China University of Petroleum, Qingdao 266580, China
[2] College of Chemical Engineering, China University of Petroleum, Qingdao 266580, China

Received: 5 June 2017
Accepted: 4 July 2017
Published online: 11 July 2017

ABSTRACT

A three-dimensional (3D) nickel oxide (NiO) catalytic electrode was fabricated by annealing Ni_2(L-asp)$_2$bipy MOF membrane and was subsequently applied for electrochemical glucose sensor. This 3D self-supported MOF membrane precursor provided uniform and porous architecture, and it was used for fabricating 3D NiO electrode in the first time. The SEM and XRD data showed that the NiO was evenly distributed on Ni mesh and complete transformation from Ni_2(L-asp)$_2$bipy to NiO. This catalytic electrode, using a chronoamperometric approach, demonstrated linear range up to 400 μM with high sensitivity of 478.9 μA mM^{-1} cm^{-2} and low limit of detection of 4.34 μM. Uric acid, urea and ascorbic acid showed negligible interferences to the detection of glucose. The excellent performance of this electrode was attributed to the uniformly distributed NiO on the Ni substrate, direct electron transformation from Ni substrate to electrochemical active NiO and the porosity of such electrode design.

Introduction

The demand for fast and accurate determination of glucose is rising to meet healthcare, food analysis and environment monitoring purposes. Traditional enzymatic glucose electrochemical biosensors, based on glucose oxidase (GOx), offer high selectivity and sensitivity, but suffer from low stability and environment dependency owing to its intrinsic nature [1]. On the other hand, non-enzymatic electrochemical glucose sensors have drawn tremendous attentions owning to its enzyme-independent property [2]. Recent developments of non-enzymatic glucose sensors showed improved sensitivity, stability and reasonable degree of selectivity [3]. Thus, the development of electrochemical non-enzymatic glucose sensor is of essential for fabricating the next generation of glucose sensor.

Address correspondence to E-mail: kangzixi69@126.com

DOI 10.1007/s10853-017-1349-2

Transition metal oxides (such as CuO, NiO, $NiMoO_4$, Co_3O_4) have been widely used as electrode materials for non-enzymatic electrochemical glucose sensors attributed to their electrochemical redox process, which can subsequently oxidize glucose, thus resulting in an enhanced current signal [4–8]. Among them, Ni-based electrode appeared to be an excellent candidate with high sensitivity [2, 9–11]. However, the synthesis of catalytic materials and the immobilization process to attach the electrochemical active materials onto electrode surface are usually separate. The immobilization process was often assisted by the introduction of organic binders, which can cause reduced intrinsic conductivity between the redox active materials and electrode surface. Therefore, the in situ growth of electrode materials onto electrode in one-step is highly desired in order to achieve high-performance glucose sensors [12–14].

Metal–organic frameworks (MOFs) have been widely applied in membrane- and film-based applications owing to its designable porous environment and variable framework [15, 16]. The direct growth of MOFs on three-dimensional (3D) conductive substrates inspired us for designing catalytic electrode for glucose sensing. Indeed, MOF as a precursor for fabricating transition metal oxides has been recently applied for constructing electrode materials for sensing applications. For instance, Hou et al. used MOF template to synthase Co_3O_4 nanoparticles for glucose and H_2O_2 detection [17], Zhou et al. introduced Cu(II)-based MOF immobilized on multiwall carbon nanotubes for H_2O_2 determination [18], Wu et al. constructed a MOF-derived Cu_2O/CuO@rGO for H_2O_2 sensing [19], and Song's group developed a sensitive H_2O_2 sensor based on Cu-Hemin MOF/chitosan-rGO nanocomposites [20]. Furthermore, the porous MOF was also applied for encapsulation of Cu nanoparticles for glucose sensing [21]. However, the functional electrode based on porous MOF membrane for monitoring glucose has not yet been reported. In our previous work, Ni_2(L-asp)$_2$bipy MOF has been successfully grown on nickel mesh to form a continuous grown MOF membrane for gas and liquid separation [22]. In this work, MOF membrane was annealed to form a uniform and porous NiO layer adhered to nickel mesh, which was directly used as catalytic electrode for monitoring glucose concentration. This catalytic electrode possessed a satisfied amperometric glucose sensor with reasonable sensitivity and low detection limit.

Experimental

Materials

Nickel carbonate basic ($NiCO_3{\cdot}2Ni(OH)_2{\cdot}4H_2O$, $NiCO_3$), methanol, bidentate aromatic nitrogen donor 4,4′-bipyridine (bipy) and L-Aspartic acid ($NH_2CH(COOH)CH_2COOH$, L-asp) were used as received. Nickel mesh (180 mesh, Xinxiang City, 540 Equipment Co., China) was used as supports. The nickel mesh was first cut into circular wafers (20 mm in diameter). Then, they were washed with ethanol and deionized water under ultrasound to clean the surface. Finally, these wafers were dried in an oven at 100 °C for 5 h at least.

Structural characterization

Powder X-ray diffraction (PXRD) was used to analyze the crystalline structures of the samples which was equipped with Philips X'Pert diffractometer with Cu Kα radiation source ($\lambda = 0.15{,}418$ nm). Scanning electron microscopy (SEM) images were collected using a Hitachi S-4800 field emission scanning electronic microscopy (FE-SEM).

Preparation of Ni(L-asp)$(H_2O)_2{\cdot}H_2O$ (Ni(L-Asp))

L-asp acid (2.63 g, 19.8 mmol) was first dissolved in 200 ml water. When this solution was heated to 100 °C, $NiCO_3$ (2.86 g, 7.61 mmol) was added. The solution was evaporated at 100 °C to prepare the $Ni(C_4O_4H_5N)(H_2O)_2{\cdot}H_2O$ (Ni(L-asp)) powders.

Preparation of MOF membranes on nickel screens and mesoporous NiO electrode

Nickel mesh served as the nickel precursor, which reacts with L-asp and bipy to produce a seed layer. 0.1 g (0.75 mmol) of L-asp was dissolved in a mixture containing 2 mL of methanol (62.4 mmol) and 0.2 mL of water (11.1 mmol). To this solution, 0.0586 g of bipy (0.375 mmol) was added and stirred for 1 h. A nickel mesh and the final mixture with a composition of 1.0 L-asp: 0.5bipy: $15H_2O$: $83CH_3OH$

were sealed into a reaction kettle and heated at 150 °C for 24 h. After this process, a seed layer was grown on the surface of the nickel mesh. Then, the seeded nickel mesh was placed vertically in a reaction kettle, in which the composition of the reaction solution was 1.0bipy: 0.9Ni(L-asp): 333H_2O: 263CH_3OH, for secondary growth at 150 °C for 2 days. The MOF membrane was then annealed at 500 °C for 2 h under in atmosphere to obtain the 3D NiO layer electrode. A schematic cartoon of preparation procedure is shown in Scheme 1 in "Results and discussion" section.

Electrochemical measurement

The electrochemical analysis was conducted on a CHI 660E electrochemical workstation. Three-electrode configuration was used, with Pt plate served as a counter electrode, saturated calomel electrode served as reference electrode and the 3D mesoporous NiO membrane served directly as working electrode. The measurements were taken in 0.1 M NaOH solution, and 0.6 cm^2 of 3D NiO electrode was immersed in the electrolyte solution.

Results and discussion

Structural characterization of MOF membrane and 3D NiO electrode

The Ni_2(L-asp)$_2$bipy membrane was fabricated by a seeding-secondary growth method as reported previously [22]. The general synthesis procedure of 3D NiO electrode from Ni_2(L-asp)$_2$bipy membrane is shown in Scheme 1. The structure information was collected by PXRD as shown in Fig. 1a. From the patterns, we can learn that no different peak appeared compared with simulated one, which proved a pure phase of Ni_2(L-asp)$_2$bipy obtained after the membrane was prepared. The MOF membrane was then annealed at 500 °C for 2 h under in atmosphere to afford 3D NiO layer electrode. The PXRD results of the black layer confirmed the NiO coating on the surface of nickel mesh (Fig. 1b).

The morphology of Ni_2(L-asp)$_2$bipy membrane was characterized by SEM technique. The top-view SEM image of MOF membrane (Fig. 2a, b) suggests the defect-free polycrystalline was successfully prepared by solvothermal process. The uniform coating of Ni-based MOF membrane gave an ideal precursor

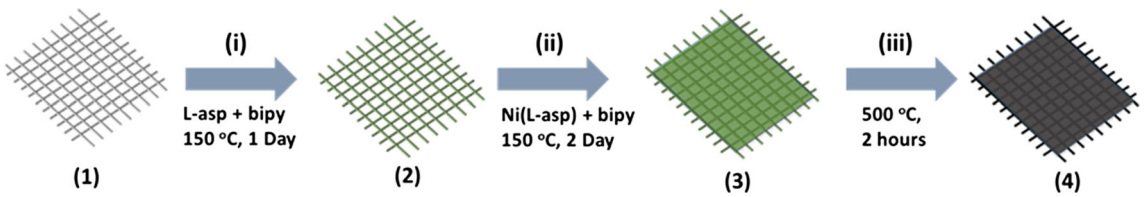

Scheme 1 A schematic cartoon illustration of preparation procedure of 3D NiO electrode from MOF membrane.

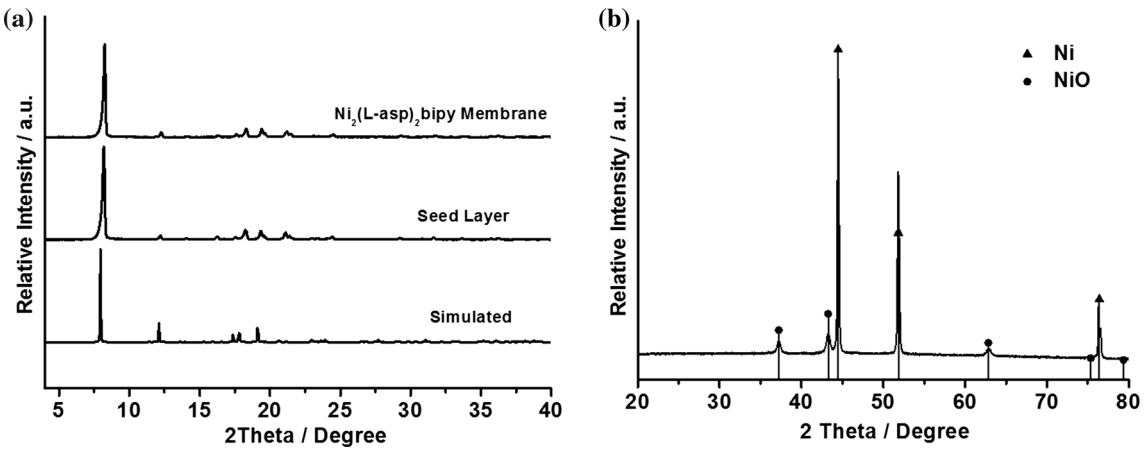

Figure 1 PXRD patterns of Ni_2(L-asp)$_2$bipy membrane (**a**) and annealed membrane (**b**).

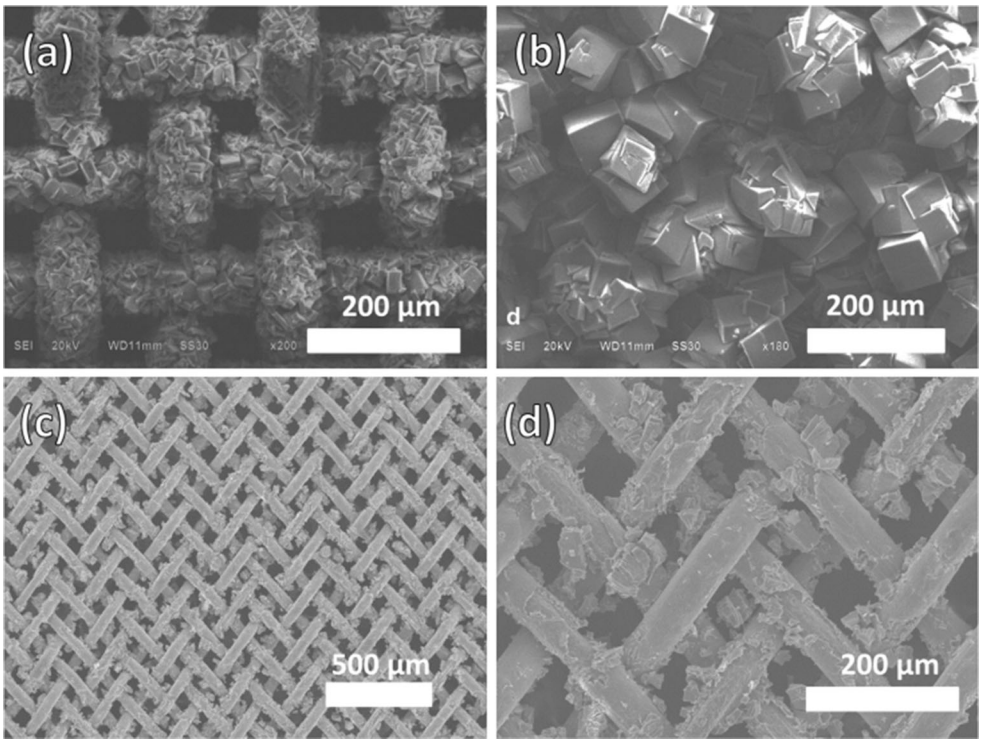

Figure 2 SEM images of seeded nickel mesh (**a**), Ni_2(L-asp)$_2$bipy membrane (**b**) and annealed membrane (**c**, **d**).

to prepare well dispersed NiO layer on supporting substrate with adhesion. After the heating treatment of step 3 in Scheme 1, the blue–green MOF membrane was conversed to black NiO particles. As illustrated in Fig. 2c, d, the NiO particles were evenly distributed on the surface of nickel meshes, which is beneficial for the accurate detection of glucose and easy to operate.

Electrochemical characterization of NiO 3D electrode

In order to achieve the electrochemical catalytic process of glucose, NiO needs to be converted (activated) into high-valent nickel oxyhydroxide (NiOOH) before it can be applied to catalyze the oxidation of glucose. Figure S1 shows the cyclic voltammograms (CV) of NiO 3D electrode after 1, 400, 800, 1200, 1600 and 2000 cycles. The oxidation peak at ca. +0.5 V versus SCE is attributed to the oxidation of Ni^{2+} to Ni^{3+}, and the corresponding reduction peak can be found at ca. +0.35 V versus SCE. In alkali solution, NiO can be electrochemically oxidized to NiOOH via the overall Eq 1. It is worth mentioning that this reaction can be divided into two elementary steps: $NiO \rightarrow Ni(OH)_2$ (hydrolyzed) and $Ni(OH)_2 \rightarrow NiOOH$ [23]. Therefore, the increase in peak current in Fig. S1 after consecutive cycles is attributed to the growth of hydroxide layer which is originated from the potential cycling [24]. In addition, negligible increase in peak current after 2000 cycles indicates that hydrolyzed $Ni(OH)_2$ had reached the maximum amount on the electrode surface, and it was readily applied for electrochemical catalytic reaction for glucose oxidation.

$$2NiO + 3OH^- \rightleftharpoons 2NiOOH + H_2O + 3e^-. \quad (1)$$

Since the catalytic active species is NiOOH and $Ni(OH)_2$, therefore it is necessary to examine the valence of Ni and O. Figure 3 shows the XPS spectrum of NiO 3D electrode before and after activation in NaOH for 2000 CV cycles. Figure 3a shows the typical Ni 2p region before the electrode was activated. The peaks at 854.10 and 872.26 eV in Fig. 3a are corresponding to the Ni^{2+} $2p_{3/2}$ and $2p_{1/2}$ orbitals, which can be attributed to the presence of NiO or $Ni(OH)_2$. The bands at 855.89 and 874.36 eV in Fig. 3a can be assigned to the Ni^{3+} $2p_{3/2}$ and $2p_{1/2}$ orbitals. The co-existence of Ni^{2+} and Ni^{3+} is commonly observed when fabricating nickel oxides [25–28].

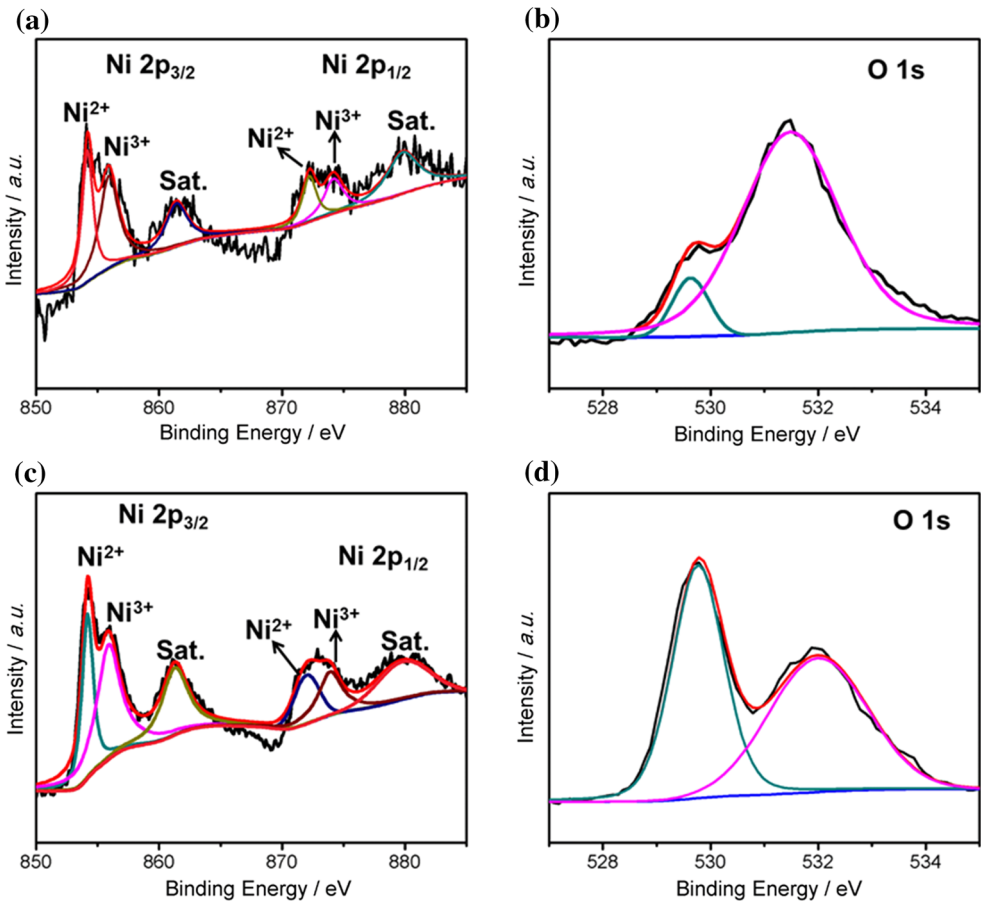

Figure 3 The XPS spectra of Ni 2p (**a**, **c**) and O 1 s (**b**, **d**) region of the 3D electrode before (**a**, **b**) and after (**c**, **d**) activated in 0.1 M NaOH.

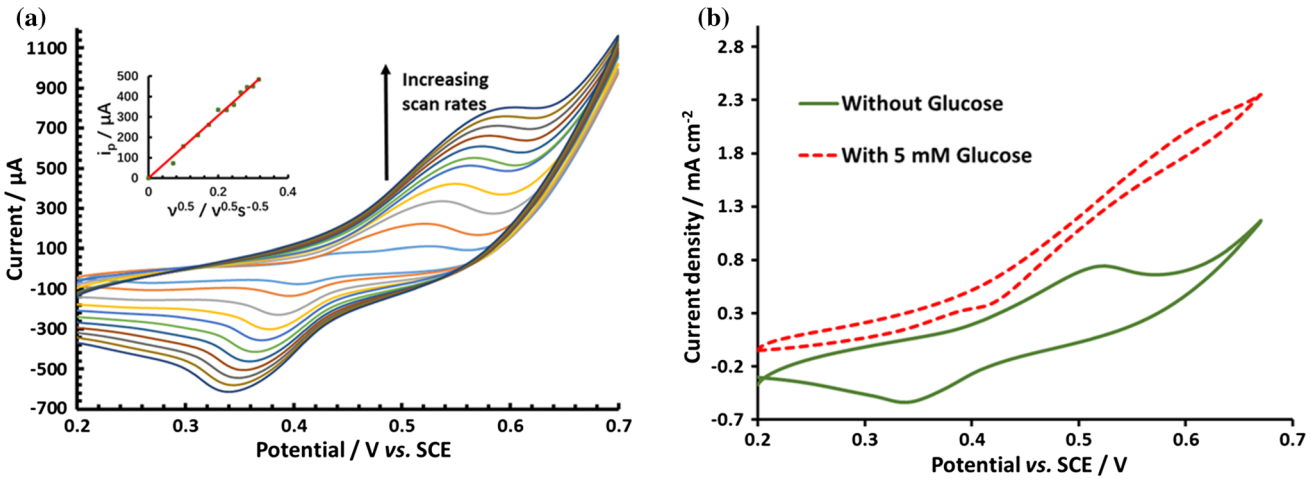

Figure 4 **a** CVs of NiO after 2000 consecutive cycles in 0.1 M NaOH at variable scan rates. **b** The CVs of NiO after 2000 consecutive cycles in 0.1 M NaOH with (*red dash line*) and without (*green solid line*) addition of 5 mM glucose.

Figure 3b shows the O 1 s region and two typical peaks can be convoluted. The peak at 529.76 eV can be assigned to the oxygen–metal bond and the peak at 531.80 eV can be attributed to hydroxyl oxygens and contaminates [25]. In comparison, after the electrode was activated, the spectrum of Ni 2p region remained similar to that of before activation (Fig. 3c). However, the peak at 529.75 eV in Fig. 3d

dramatically increased after the electrode was cycled in NaOH. This can be attributed to the formation of NiOOH on the electrode surface causing the increased signal of metal–oxygen bond [25].

The insight of electrochemical behavior of 3D NiO electrode (the electrochemical oxidation of $Ni(OH)_2$) was further characterized. Figure 4a shows the CV of 3D NiO electrode (the oxidation of $Ni(OH)_2$ to be more precise) at variable scan rates (ν). According to Randles–Sèvick equation, the corresponding peak current against square root of scan rate was plotted and is shown in the insertion of Fig. 4a. The linear relationship suggesting the electrode process is limited by diffusion. This is reasonable since the electrochemical oxidation of $Ni(OH)_2$ to NiOOH coupled with OH^-, which was diffused to the electrode surface from the bulk electrolyte solution. As shown in Fig. 4b, upon the addition of 5 mM glucose, the peak current dramatically increased. The tendency of the CV shape toward sigmoidal shape indicates that the glucose is electrocatalytically oxidized via an EC′ mechanism as shown in Scheme 2.

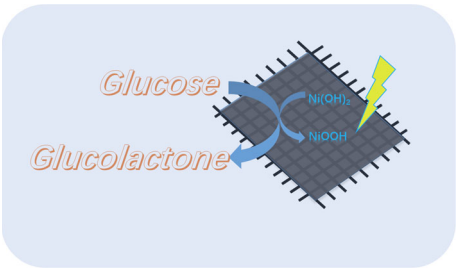

Scheme 2 A schematic diagram of electrochemical process of NiO catalyzed glucose oxidation.

The electrochemical determination of glucose at 3D NiO electrode was performed by chronoamperometric approach. The electrode potential was held at +0.5 V versus SCE. As shown in Fig. 5a, upon the addition of glucose, the anodic current increases significantly. The potential of +0.5 V versus SCE was chosen according to the CV diagram, that is, the potential at the beginning of oxidation of Ni^{2+} to Ni^{3+}. The potentials of +0.4 V and +0.6 V versus SCE were also tested, shown in Fig. S2. It is obvious that the potential at +0.4 V versus SCE does not provide sufficient signal responses upon the addition of same amount of glucose, whereas the potential at +0.6 V versus SCE provides the similar current response, but the initial current density begins at ca. 300 μA cm^{-2}, which may significantly affect the current response. Therefore, the static potential at +0.5 V versus SCE was found to be the optimal condition. Figure 5b shows the corresponding calibration curve of the glucose sensor. The linearity range of glucose response was determined up to 400 μM, with a sensitivity of 478.9 μA mM^{-1} cm^{-2}. The detection limit of such method was determined to be 4.34 μM at signal-to-noise (S/N) ratio of 3. Sensitivity and detection limit were comparable with other literature reports as shown in Table 1.

Interference tests are essential for the evaluation of glucose sensor since other bio-organic molecules may interfere with the current response at real circumstances. Figure 6 shows the interference test using the same potential static method. Again, the potential was held at +0.5 V versus SCE and the addition of 0.1 mM glucose causes significant current response up to 32 μA. After the addition of 0.1 mM glucose, 0.01 mM urea, 0.01 mM uric acid and 0.01 mM

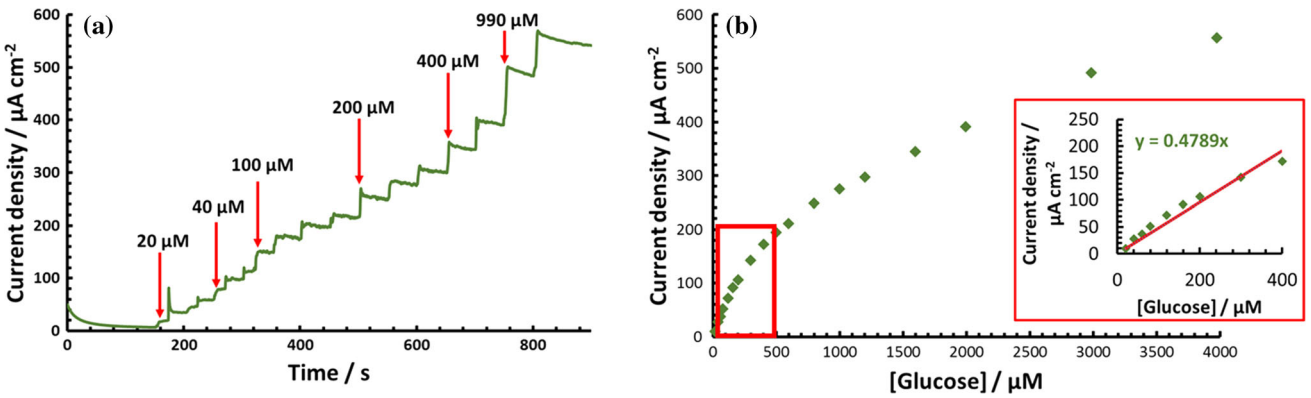

Fig. 5 Amperometric response of 3D NiO electrode with successive addition of glucose in 0.1 M NaOH at +0.5 V versus SCE. **b** The corresponding calibration plot of graph (**a**). The insertion of (**b**) shows the linear region of the calibration graph.

Table 1 Analytical performance of 3D NiO electrode in comparison with other metal-oxide-based non-enzymatic glucose sensors

Electrode material	Sensitivity (μA mM^{-1} cm^{-2})	Limit of detection (μM)	References
NiO/graphene	666.71	5	Zeng et al. [29]
CS/RGO/NiNPs	318.4	4.1	Yang et al. [30]
MWCNT/NiO	436	160	Shamsipur et al. [31]
Ni/TiO_2	50.97	0.18	Xu et al. [32]
NiO/CuO/polyaniline	340.2	2	Ghanbari and Babaei [33]
Cu_2O/TiO_2 nanotube	14.56	62	Long et al. [34]
Cu_2O/CQD	298	8.4	Li et al. [35]
N-Co-CNT@NG	9.05	2.0	Balamurugan et al. [36]
Fe_3O_4-CNTs-NiNPs	335.25	6.7	Nontawong et al. [37]
3D NiO electrode	478.9	4.3	This work

CS chitosan, *RGO* reduced graphene oxide, *NPs* nanoparticles, *MWCNT* multiwall carbon nanotube, *CQD* carbon quantum dot, *N-Co-CNT@NG* nitrogen-doped Co-CNTs over graphene sheets, *CNTs* carbon nanotubes

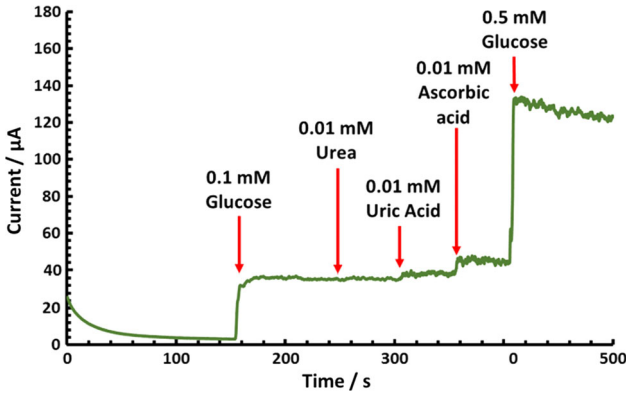

Fig. 6 Interference test of 3D NiO electrode 0.1 M NaOH at +0.5 V versus SCE.

ascorbic acid were added subsequently. Negligible current responses were detected after the addition of urea and uric acid. The addition of ascorbic acid causes slight increase in current, which can be attributed to the catalytic oxidation of ascorbic acid. The current signal of ascorbic acid is much weaker than glucose since the former requires higher oxidation potential. It is worth mentioning that the concentration of interferences was ten times less than that of glucose, which is reasonable since the concentration of those interferences in plasma is roughly ten times less than that of glucose [38]. Accordingly, this glucose sensor offers reasonable selectivity. After the addition of interferences, 0.5 mM glucose was added in the system and a large current increase appeared again, suggesting good reproducibility of such glucose sensor.

Conclusion

In conclusion, the 3D NiO glucose sensor was fabricated from thermal annealing of Ni_2(L-asp)$_2$bipy MOF membrane. This in situ thermally treated 3D electrode inherited the even distribution of electrochemical active species, high porosity and direct electron transfer from Ni mesh to NiO. This electrode showed excellent performances toward amperometric detection of glucose, with linear range up to 400 μM, high sensitivity of 478.9 μA mM^{-1} cm^{-2} and low limit of detection of 4.34 μM. Furthermore, the existence of urea, uric acid and ascorbic acid showed negligible interferences to the glucose responses. These results demonstrated that the 3D NiO electrode prepared from MOF membrane is a competitive candidate for non-enzymatic detection of glucose.

Acknowledgements

The authors thank for the financial supports provided by National Natural Science Foundation of China (21501198).

Electronic supplementary material: The online version of this article (doi:10.1007/s10853-017-1349-2) contains supplementary material, which is available to authorized users.

References

[1] Park S, Boo H, Chung TD (2006) Electrochemical non-enzymatic glucose sensors. Anal Chim Acta 556:46–57

[2] Toghill KE, Compton RG (2010) Electrochemical non-enzymatic glucose sensors: a perspective and an evaluation. Int J Electrochem Sci 5:1246–1301

[3] Niu XH, Li X, Pan JM, He YF, Qiu FX, Yan YS (2016) Recent advances in non-enzymatic electrochemical glucose sensors based on non-precious transition metal materials: opportunities and challenges. Rsc Adv 6:84893–84905

[4] Ensafi AA, Ahmadi N, Rezaei B (2017) Nickel nanoparticles supported on porous silicon flour, application as a non-enzymatic electrochemical glucose sensor. Sens Actuators B Chem 239:807–815

[5] Garcia-Garcia FJ, Salazar P, Yubero F, Gonzalez-Elipe AR (2016) Non-enzymatic Glucose electrochemical sensor made of porous NiO thin films prepared by reactive magnetron sputtering at oblique angles. Electrochim Acta 201:38–44

[6] Khedekar VV, Bhanage BM (2016) Simple electrochemical synthesis of cuprous oxide nanoparticles and their application as a non-enzymatic glucose sensor. J Electrochem Soc 163:B248–B251

[7] Mahmoudian MR, Basirun WJ, Woi PM, Sookhakian M, Yousefi R, Ghadimi H, Alias Y (2016) Synthesis and characterization of Co_3O_4 ultra-nanosheets and Co_3O_4 ultra-nanosheet-Ni(OH)(2) as non-enzymatic electrochemical sensors for glucose detection. Mater Sci Eng C Mater Biol Appl 59:500–508

[8] Wang D, Cai D, Huang H, Liu B, Wang L, Liu Y, Li H, Wang Y, Li Q, Wang T (2015) Non-enzymatic electrochemical glucose sensor based on NiMoO4 nanorods. Nanotechnology 26:145501

[9] Deng Z, Long H, Wei Q, Yu Z, Zhou B, Wang Y, Zhang L, Li S, Ma L, Xie Y, Min J (2017) High-performance non-enzymatic glucose sensor based on nickel-microcrystalline graphite-boron doped diamond complex electrode. Sens Actuators B Chem 242:825–834

[10] Wang L, Lu X, Wen C, Xie Y, Miao L, Chen S, Li H, Li P, Song Y (2015) One-step synthesis of Pt–NiO nanoplate array/reduced graphene oxide nanocomposites for nonenzymatic glucose sensing. J Mater Chem A 3:608–616

[11] Wang L, Zhang Y, Yu J, He J, Yang H, Ye Y, Song Y (2017) A green and simple strategy to prepare graphene foam-like three-dimensional porous carbon/Ni nanoparticles for glucose sensing. Sens Actuators B Chem 239:172–179

[12] Song Y, Liu H, Tan H, Xu F, Jia J, Zhang L, Li Z, Wang L (2014) pH-switchable electrochemical sensing platform based on chitosan-reduced graphene oxide/concanavalin a layer for assay of glucose and urea. Anal Chem 86:1980–1987

[13] Song Y, Lu X, Li Y, Guo Q, Chen S, Mao L, Hou H, Wang L (2016) Nitrogen-doped carbon nanotubes supported by macroporous carbon as an efficient enzymatic biosensing platform for glucose. Anal Chem 88:1371–1377

[14] Wang L, Zhang Q, Chen S, Xu F, Chen S, Jia J, Tan H, Hou H, Song Y (2014) Electrochemical sensing and biosensing platform based on biomass-derived macroporous carbon materials. Anal Chem 86:1414–1421

[15] Adatoz E, Avci AK, Keskin S (2015) Opportunities and challenges of MOF-based membranes in gas separations. Sep Purif Technol 152:207–237

[16] Zhang Y, Feng X, Yuan S, Zhou J, Wang B (2016) Challenges and recent advances in MOF-polymer composite membranes for gas separation. Inorg Chem Front 3:896–909

[17] Hou C, Xu Q, Yin L, Hu X (2012) Metal-organic framework templated synthesis of Co_3O_4 nanoparticles for direct glucose and H_2O_2 detection. Analyst 137:5803–5808

[18] Zhou E, Zhang Y, Li Y, He X (2014) Cu(II)-based MOF immobilized on multiwalled carbon nanotubes: synthesis and application for nonenzymatic detection of hydrogen peroxide with high sensitivity. Electroanalysis 26:2526–2533

[19] Wu D, Xu Z, Zhang T, Shao Y, Xi P, Li H, Xu C (2016) Cu_2O/CuO@rGO heterostructure derived from metal-organic-frameworks as an advanced electrocatalyst for non-enzymatic electrochemical H_2O_2 sensor. RSC Adv 6:103116–103123

[20] Wang L, Yang H, He J, Zhang Y, Yu J, Song Y (2016) Cu-hemin metal-organic-frameworks/chitosan-reduced graphene oxide nanocomposites with peroxidase-like bioactivity for electrochemical sensing. Electrochim Acta 213:691–697

[21] Shi L, Zhu X, Liu T, Zhao H, Lan M (2016) Encapsulating Cu nanoparticles into metal-organic frameworks for nonenzymatic glucose sensing. Sens Actuators B Chem 227:583–590

[22] Kang Z, Xue M, Fan L, Huang L, Guo L, Wei G, Chen B, Qiu S (2014) Highly selective sieving of small gas molecules by using an ultra-microporous metal-organic framework membrane. Energy Environ Sci 7:4053–4060

[23] Wang S, Wang C, Wei G, Xiao H, An N, Zhou Y, An C, Zhang J (2016) Non-enzymatic glucose sensor based on facial hydrothermal synthesized NiO nanosheets loaded on glassy carbon electrode. Colloids Surf A 509:252–258

[24] Medway SL, Lucas CA, Kowal A, Nichols RJ, Johnson D (2006) In situ studies of the oxidation of nickel electrodes in alkaline solution. J Electroanal Chem 587:172–181

[25] Xu K, Huang X, Liu Q, Zou R, Li W, Liu X, Li S, Yang J, Hu J (2014) Understanding the effect of polypyrrole and poly(3,4-ethylenedioxythiophene) on enhancing the

supercapacitor performance of $NiCo_2O_4$ electrodes. J Mater Chem A 2:16731–16739

[26] Zhao Y, Wang Q, Bian T, Yu H, Fan H, Zhou C, Wu LZ, Tung CH, O'Hare D, Zhang T (2015) Ni^{3+} doped monolayer layered double hydroxide nanosheets as efficient electrodes for supercapacitors. Nanoscale 7:7168–7173

[27] Gao S, Liao F, Ma S, Zhu L, Shao M (2015) Network-like mesoporous $NiCo_2O_4$ grown on carbon cloth for high-performance pseudocapacitors. J Mater Chem A 3:16520–16527

[28] Parveen N, Cho MH (2016) Self-assembled 3D flower-like nickel hydroxide nanostructures and their supercapacitor applications. Sci Rep 6:27318

[29] Zeng G, Li W, Ci S, Jia J, Wen Z (2016) Highly dispersed NiO nanoparticles decorating graphene nanosheets for non-enzymatic glucose sensor and biofuel cell. Sci Rep 6:36454

[30] Yang J, Yu J-H, Rudi Strickler J, Chang W-J, Gunasekaran S (2013) Nickel nanoparticle–chitosan-reduced graphene oxide-modified screen-printed electrodes for enzyme-free glucose sensing in portable microfluidic devices. Biosens Bioelectron 47:530–538

[31] Shamsipur M, Najafi M, Hosseini M-RM (2010) Highly improved electrooxidation of glucose at a nickel(II) oxide/multi-walled carbon nanotube modified glassy carbon electrode. Bioelectrochemistry 77:120–124

[32] Xu J, Xu N, Zhang X, Xu P, Gao B, Peng X, Mooni S, Li Y, Fu J, Huo K (2017) Phase separation induced rhizobia-like Ni nanoparticles and TiO_2 nanowires composite arrays for enzyme-free glucose sensor. Sens Actuators B Chem 244:38–46

[33] Ghanbari K, Babaei Z (2016) Fabrication and characterization of non-enzymatic glucose sensor based on ternary NiO/CuO/polyaniline nanocomposite. Anal Biochem 498:37–46

[34] Long M, Tan L, Liu H, He Z, Tang A (2014) Novel helical TiO_2 nanotube arrays modified by Cu_2O for enzyme-free glucose oxidation. Biosens Bioelectron 59:243–250

[35] Li Y, Zhong Y, Zhang Y, Weng W, Li S (2015) Carbon quantum dots/octahedral Cu_2O nanocomposites for non-enzymatic glucose and hydrogen peroxide amperometric sensor. Sens Actuators B Chem 206:735–743

[36] Balamurugan J, Thanh TD, Karthikeyan G, Kim NH, Lee JH (2017) A novel hierarchical 3D N-Co-CNT@NG nanocomposite electrode for non enzymatic glucose and hydrogen peroxide sensing applications. Biosens Bioelectron 89:970–977

[37] Nontawong N, Amatatongchai M, Jarujamrus P, Tamuang S, Chairam S (2017) Non-enzymatic glucose sensors for sensitive amperometric detection based on simple method of nickel nanoparticles decorated on magnetite carbon nanotubes modified glassy carbon electrode. Int J Electrochem Sci 12:1362–1376

[38] Krebs HA (1950) Chemical composition of blood plasma and serum. Annu Rev Biochem 19:409–430